INTERNATIONAL ATOMIC ENERGY AGENCY
UNITED NATIONS EDUCATIONAL, SCIENTIFIC AND CULTURAL ORGANIZATION
INTERNATIONAL CENTRE FOR THEORETICAL PHYSICS
I.C.T.P., P.O. BOX 586, 34100 TRIESTE, ITALY. CABLE CENTRATOM TRIESTE

IN REPLY PLEASE REFER TO

SMR. 758 - 6

SPRING COLLEGE IN CONDENSED MATTER
ON QUANTUM PHASES
(3 May - 10 June 1994)

==========

FURTHER BACKGROUND MATERIAL for lectures on

OPTICAL AND TRANSPORT STUDIES ACROSS THE METAL-INSULATOR TRANSITION

Gordan THOMAS
AT&T Bell Laboratories
Murray Hill, NJ 07974-9636, U.S.A.

==========

These are preliminary lecture notes, intended only for distribution to participants.

==========

HIGH TEMPERATURE SUPERCONDUCTIVITY

Proceedings of the Thirty-Ninth Scottish
Universities Summer School in Physics,
St Andrews, June 1991.

A NATO Advanced Study Institute.

Edited by

D P Tunstall - St Andrews University
W Barford - Sheffield University

Series Editor

P Osborne - Edinburgh University

Copublished by
Scottish Universities Summer School in Physics &
Adam Hilger, Bristol, Philadelphia and New York

Optical Properties of Insulators and Metals with Copper Oxide Planes

G A Thomas

AT & T Bell Laboratories
Murray Hill, New Jersey

1 Introduction

The motivation for the optical studies of materials containing Cu-O planes has been to try to understand high temperature superconductivity (Bednorz, 1986; Cava, 1987; Wu, 1987 and Takagi, 1989). The experiments discussed here are presented here primarily as measurements of the electrical conductivity σ as a function of four 'variables':

1. the charge density added by doping: n.
2. the lattice structure (different materials with Cu-O planes).
3. the temperature of the crystals: T.
4. the energy of the photons used as a probe: E or ω.

In this article we wish to reframe some of the question currently being asked about high temperature superconductors. In Section 2 we shall look at the range of materials involved and in Sections 3, 4, 5 we shall look at their insulating, metallic and superconducting states respectively. Note that this article is not intended to be a comprehensive review, and the references given are only examples in which a reader can find some discussion of the subjects cited.

A few units involved in these variables are useful to have at hand;

$$\begin{array}{lrcll} T\text{:} & 1\ \text{K} & = & 0.0862\text{meV} & = 0.695\text{cm}^{-1} \\ E\text{:} & 1\ \text{meV} & = & 11.6\text{K} & = 8.066\text{cm}^{-1} \quad = 2.419 \times 10^{11}\text{sec}^{-1} \\ \omega\text{:} & 1\ \text{cm}^{-1} & = & 1.44\ \text{K} & = 0.124\text{meV} \end{array}$$

2 Materials

We shall concentrate on optical studies of crystals and crystalline films, and ignore studies of pressed pellets and textured ceramics in which many small crystals are not aligned with each other [reviewed along with results from some crystals in Timusk (1989)]. The conductivity within the Cu–O planes is qualitatively different from that perpendicular to them (Batlogg, 1990 and Timusk, 1989). For most purposes, this anisotropy adds an extra complexity for unaligned crystals. We interpret the conductivity along the two planar axes (a, b) as qualitatively similar (Pham, 1990 and Welp, 1990), so we shall consider both twinned (a axes of different crystals not aligned) and single domain crystals.

The principal issue related to the materials is the extent of their disorder. Can we learn from disordered crystals? When is macroscopic homogeneity a reasonable approximation? Should some samples be regarded as made up of two (or more) compositions. This case would require a special analysis (such as percolation theory). Alternatively, should such materials be ignored? Should we be, at least, highly sceptical of all measurements of materials that are not stoichiometric compounds?

Some stoichiometric compounds:

$$\left.\begin{array}{ll} \text{YBCO} & (90K \text{ or } 0K) \\ \text{NCO} & (y = 0) \end{array}\right\} \text{ assumed homogeneous}$$

We shall sometimes use abbreviations for the materials:

YBCO(T_c)	=	$YBa_2Cu_3O_{6+y}$, with T_c specified (doped with interstitial O)
NCO(y)	=	Nd_2CuO_{4-y}, with y specified (vacancies)
LCO(y)	=	La_2CuO_{4+y}, (interstitial O)
LSCO(x)	=	$La_{2-x}Sr_xCuO_{4+y}$, (substitutional Sr), y assumedzero .

Values of y are generally not well known (Batlogg, 1990). The charge density can be estimated from optical and other electrical measurements but with substantial systematic uncertainties [Thomas,1988; Timusk,1989 and Orenstein, 1990]. The charge density in the planes of YBCO is particularly problematical because substantial charge resides between them. For this reason, we use the values of T_c to specify these samples. Estimates have been made of T_c versus y (Batlogg, 1990).

Others have argued, at least implicitly, that some non-stoichiometric samples are close enough to being homogeneous that we can reasonably draw some conclusions from them [Thomas, 1988, 1991; Cooper,1989; Orenstein,1990; Uchida,1991; Suzuk,1989 and Preyer,1989]

Some doped semiconductors:

$$\left.\begin{array}{ll} \text{YBCO} & (\text{all } T_c) \\ \text{NCO} & (y = .03) \\ \text{LCO} & (y = .03) \end{array}\right\} \text{ assumed macroscopically homogeneous}$$

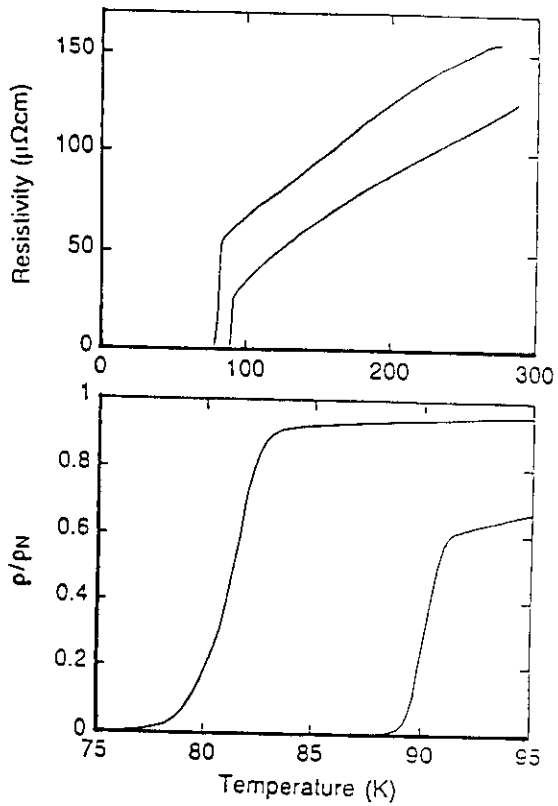

Figure 1: *Resistivity (inverse conductivity) in the Cu–O plane at zero frequency for two crystals of* YBCO *with different values of charge density (specified by values of T_c:* YBCO *(90K) and* YBCO *(80K)) as a function of temperature (T). (Measurements by Martin, published by Orenstein, 1990).*

That non-stoichiometric crystals are sometimes not satisfactorily homogeneous is perhaps obvious. Some indications include non-reproducibility, low apparent conductivity, and low reflectivity in the superconducting state [Thomas,1988]. We have no assurance that even nominally stoichiometric materials are satisfactorily homogeneous for the conclusions we wish to draw (*i.e.* good enough to support or rule out a particular interpretation).

Let us consider some evidence suggesting that there exist crystals that are approximately homogeneous on a length scale appropriate for the quantity measured. Figure 1 is the first example. The homogeneity approximation seems reasonable for both crystals in Figure 1 in that the transition from the normal to the superconducting state occurs over a narrow range of temperature. The higher resistivity and broader transition in YBCO (80K) indicate more disorder. Both crystals have low resistivity compared to others reported (Batlogg, 1990 and 1991)

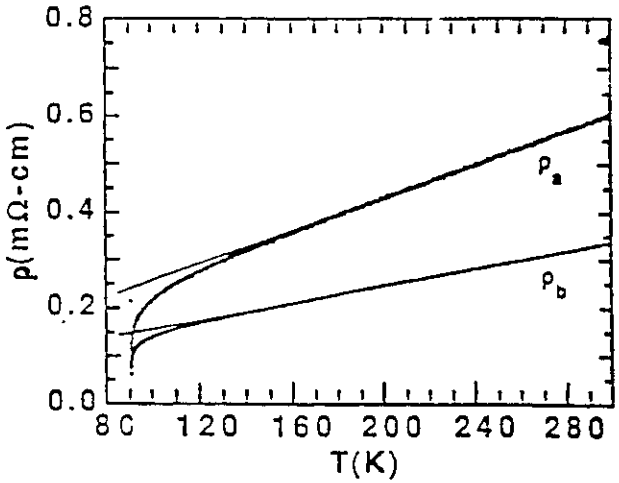

Figure 2: *Resistivity at $\omega = 0$ of* YBCO *(90K) along* a*-axis and along* b*-axis (the larger Cu–O spacing in the planes and parallel to Cu–O chains in the structure) as a function of temperature, Welp (1990).*

The disorder can be much larger (higher resistivity) and still have reasonable apparent homogeneity as, for example, in crystals of YBCO (90K) detwinned by uniaxial stress, as illustrated in Figure 2. The normal to superconducting transition occurs over a relatively narrow range of T. Crystals prepared in the same way as these have been studied optically (as discussed below) [Schlesinger,1990 and Pham,1991] and show very high reflectivity (low absorption) in the superconducting state. We interpret these characteristics as indicating good homogeneity.

The criterion for applying the approximation of macroscopic homogeneity depends on the quantity measured. The motion of the electrons averages over some length scale, L_a. In the conductivity, L_a is probably a function of the inelastic scattering length . There is disorder and inhomogeneity (spatially varying composition or defects [Phillips,1989]) over some length scale, L_d. For approximate homogeneity, the averaging must be effective (lead to the dominant measured effect) over a length larger than the disorder. Therefore, $L_a > L_d$, becomes a *homogeneity* criterion.

Microwave absorption, Figure 3, is the second example of a measurement probing approximate homogeneity in non-stoichiometric crystals. The absorption is strong where lossy motion of magnetic flux lines occurs. This effect probes different electronic motion from that involved in the resistivity, and so has a different sensitivity to homogeneity. In particular, a superconducting filament cannot short out a normal region as it can at dc. For the YBCO (90K) crystal shown in Figure 3, the normal to superconducting transition occurs over a narrow temperature region and would be considered satisfactorily homogeneous in most measurements. The YBCO (50K) crystal has a sharper transition and shows absorption only near 50K. (There is no material of size larger than L_a with a T_c of 90K.) We consider this crystal to be to a good approximation macroscopically homogeneous, although it is certainly disordered.

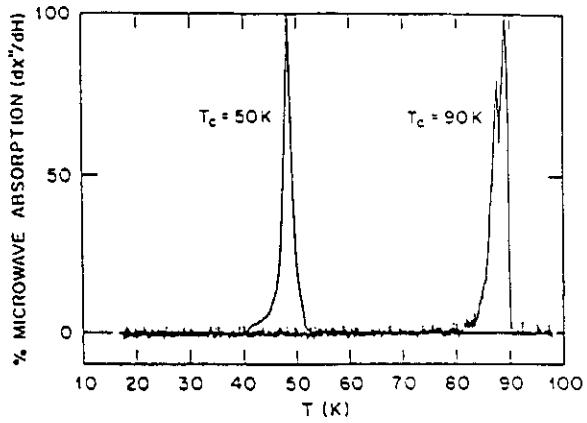

Figure 3: *Microwave absorption magnitude in* YBCO *(50K) and* YBCO *(90K) at X-band frequency (near $\omega = 0$, compared to optical measurements) as a function of temperature [Measurements by Glarum, published by Orenstein,1990].*

In the following sections we shall discuss data from samples that appear to satisfy the criteria for approximate homogeneity. We have no proof that this is the case, but we shall assume it.

3 Insulating state

The principal issue we wish to discuss is what are the excitations that show up when we add a few charges to a pure (that is undoped), insulating crystal, such as $NCO(0)$. In the pure case, some excitations are the following:

1. phonons
2. optically excited electrons and holes (interband transitions) and excitons
3. thermally excited electrons and holes
4. magnons

In other words, for pure crystals:

$$\sigma_{\text{pure}} = \sigma_{\text{phonons}} + \sigma_{\text{interband}} + \sigma_{\text{excitons}} + \sigma_{\text{free}} + \sigma_{\text{magnons}} \,. \tag{1}$$

When charges are added (for example, by doping) there are also:

5. charges bound to impurities

$$\sigma_{\text{doped}} = \sigma_{\text{pure}} + \sigma_{\text{imp}} \tag{2}$$

Let us consider the extent to which these excitations play a role in the conductivity. An example is shown in Figure 4.

The phonons are easily seen in both samples as sharp lines at low frequencies (over the range from about 100–600 cm^{-1} or 12–75 meV). These are dipole-active lattice

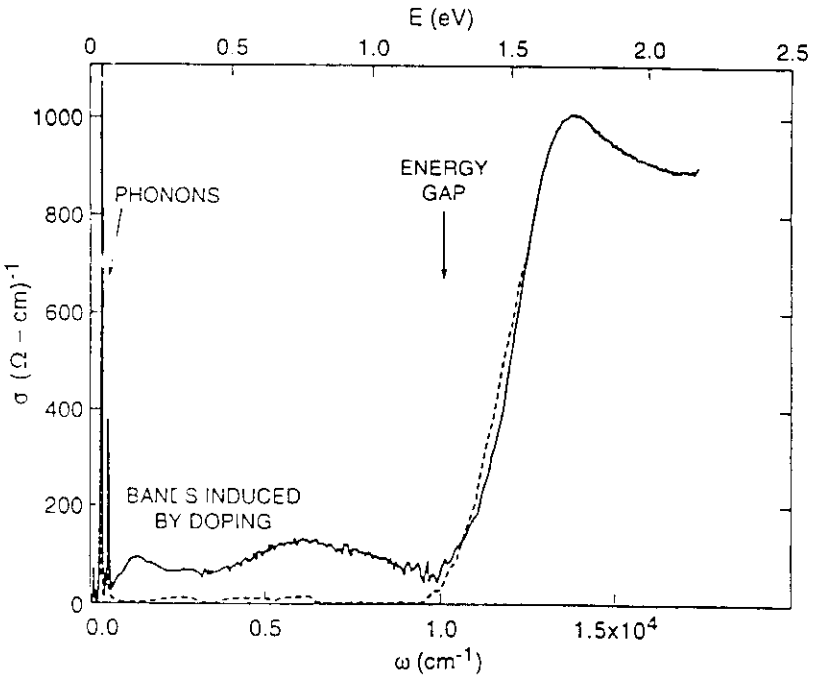

Figure 4: *Conductivity in the Cu–O plane at a low temperature ($T = 10K$) for two insulating crystals ($NCO(\sim 0)$, dashed curve and $NCO(\sim .03)$, solid curve, as a function of photon energy (upper scale) and frequency (lower scale), Thomas (1991).*

vibrations of symmetry E_u, with wave vector near zero ($\sim$ 1% to 5% of the zone boundary wave vector). The phonons change with doping (although this change cannot be seen in Figure 4) due to polaronic interactions (Mott, 1990), and new vibrations arise (sometimes called infrared active vibrational modes, IRAV) because of the near dopant sites (Mihailovic, 1988; Ginder, 1988 and Talliani, 1988).

For doped crystals, we have therefore :

$$\sigma'_{\text{phonons}} = \sigma_{\text{phonons}} + \sigma_{\text{polarons}} + \sigma_{\text{IRAV}}$$

In the insulator (Figure 4), $\sigma_{\text{polaron}}$and σ_{IRAV} are very small. At higher doping density they will increase.

The electrons and holes excited by the incident light across the semiconducting energy gap are the dominant contribution to the conductivity in Figure 4. In this excitation a photon is absorbed and a hole is created in the (filled) valence band (composed predominantly of orbitals similar to those on an oxygen atom) along with an electron in the empty conduction band (composed of Cu-like orbitals). This gap increases in Cu–O materials in which the CuO spacing is smaller [Cooper (1990)], because of an effect similar to level repulsion in atoms. (See Figure 5).

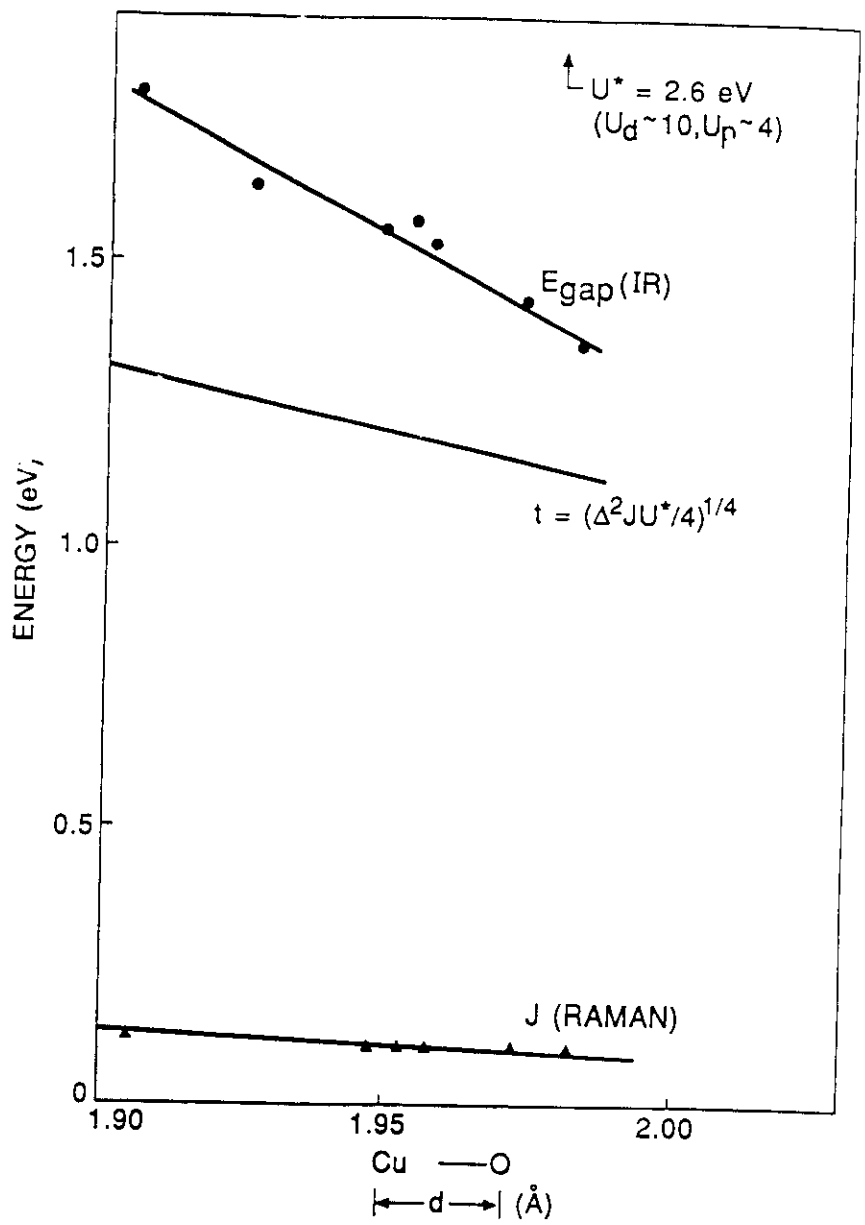

Figure 5: *Energies of insulating cuprates as a function of the Cu–O distance in the lattice planes. The semiconducting energy gap Egap (solid circles) and the super-exchange energy J (triangles) are replotted from Cooper (1990). The hopping energy t is calculated from the equation given (with $\Delta \equiv E_{gap}$).*

Again for doped crystals therefore ;

$$\sigma'_{\text{interband}} = \sigma_{\text{interband}} - \sigma_{\text{charges}} \tag{3}$$

There are no free electrons and holes at zero T in either of these samples (this is what we mean by an insulator). The number of electrons and holes excited by temperature is negligible under the conditions of Figure 4. The *dc* conductivity at $T = 10K$ is exponentially activated and less than $10^{-4}(\Omega.\text{cm})^{-1}$ [Preyer,1989 and Harshman,1988].

There is also no significant contribution to the spectrum from direct absorption by magnons. In Raman scattering, a major contribution is from creation of magnon pairs (two-magnon scattering from, which the superexchange energy J has been determined (Sulewski, 1990). See Figure 5.

The conductivity in the doped crystals is then given to a good approximation by

$$\sigma_{\text{doped}} = \sigma_{\text{phonons}} + \sigma_{\text{interband}} + \sigma_{\text{impurities}} \tag{4}$$

Figure 4 clearly shows bands induced by doping. These bands are the result we would like to emphasise primarily about the insulating state. Similar bands have been observed in at least three of the materials with Cu-O planes, as shown in Figure 6. The dashed curves in Figure 6 indicate that the conductivity added by doping can be empirically described by two contributions.

$$\sigma_{\text{impurities}} = \sigma_J + \sigma_I$$

We label these two parts J and I, based on guesses about their origin. The peak J at an energy near the antiferromagnetic exchange energy, J. A picture of a possible impurity ground state and excited state is illustrated in Figure 7. Here, the vacancy, V_{++}, binds an electron (in each plane). One excited state involves the electron hopping from one bound state to another, Rabe (1990), Shraiman (1991). This hopping is similar to that of a free charge in an antiferromagnet, von Szczepanski (1989), which is illustrated in Figure 8. The low energy, initial state of the charge will be with spin aligned with that on the site it occupies. The surrounding charges will be ordered antiferromagnetically. After the hopping is induced by an incident photon, we have the situation shown in Figure 9. The lowest energy final state is again with the electron spin aligned antiparallel to that of its site. Since the light does not flip a spin, the site from which the electron started out will have its spin misaligned compared to the surrounding antiferromagnetic order . This misalignment might account for the reduced change in energy of the hopping process.

In addition to this (polaronic) spin energy in the J transition, there is also a polaronic lattice energy (Mott,1990). The lattice around the initial site is distorted by the charge, while the final state will not distort instantaneously. The relaxation of the spin and lattice contribute to the line width of the transition.

The peak I is near a rough estimate of the ionisation energy of a charge bound to the impurity atom (Mott,1990 and Thomas,1991). In this transition (or group of transitions), the photon moves the electron from its ground state (pictured above) to the continuum (the conduction band), or a state so near by as to be indistinguishable. A sketch of the single particle density of states is shown in Figure 10.

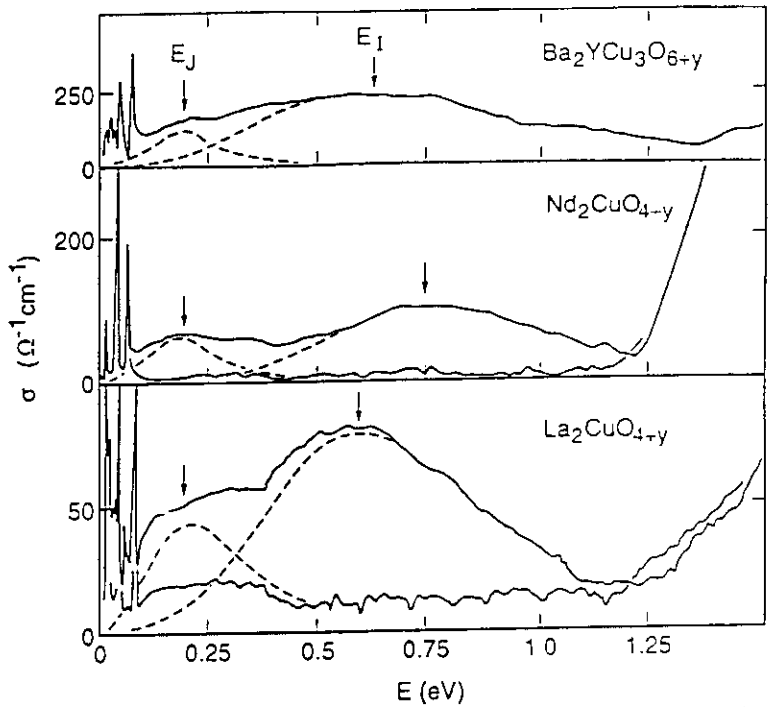

Figure 6: *Conductivity of different materials in the insulating state as a function of photon energy. The upper part shows the result for a crystal of YBCO ($0K, y \sim 0.1$) (with a small number of interstitial oxygen dopant atoms added to the pure semiconductor) measured at T=300K. The middle part shows a crystal of $NCO(\sim 0)$ (nominally undoped) as the lower curve and $NCO(0.02)$ as the upper curve, both at T=10K. The lower part shows $LCO(0.002)$ as the lower curve and $LCO(0.01)$ as the upper curve at T=10K (Thomas,1991).*

The Coulomb energy in the ground state, E_C, can be estimated simply from the impurity to Cu-O plane distance r and the local (or high frequency) dielectric constant, ϵ_L.

$$E_C = e^2/\epsilon_L r \ . \tag{5}$$

The three materials whose spectra are shown in Figure 6 have similar crystal structures (Figure 11).

In each case the dopant atoms sit between the planes. In each case, the charge (electron or hole) that is bound to the atom will reside (at lease partly) on the plane nearby. We guess that this planar charge will be the part of the electronic wave function that is most weakly bound, and will therefore give rise to the features important in the low energy spectrum. (We expect the "chain" excitations in YBCO to be at higher energy.) Table 1 summarises the relevant parameters for several materials.

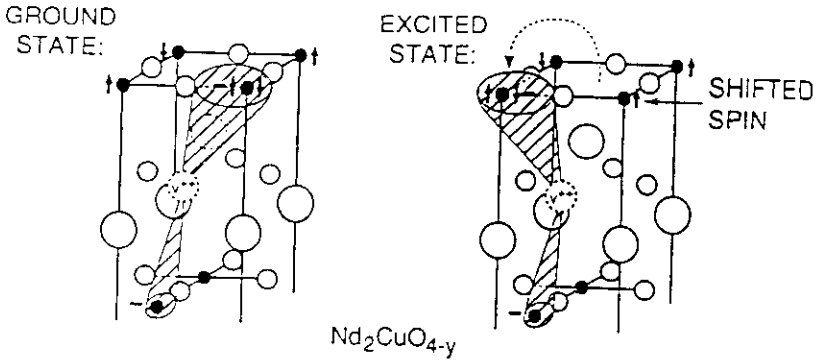

Figure 7: *Drawings of a vacancy in NCO.*

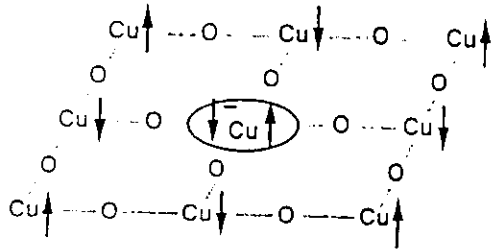

Figure 8: *Drawing of an electron in a CuO plane.*

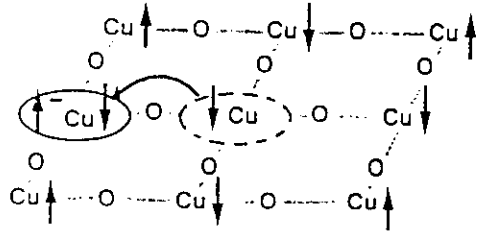

Figure 9: *Drawing of an electron that has hopped in a CuO plane, with the spins not yet relaxed after the hopping.*

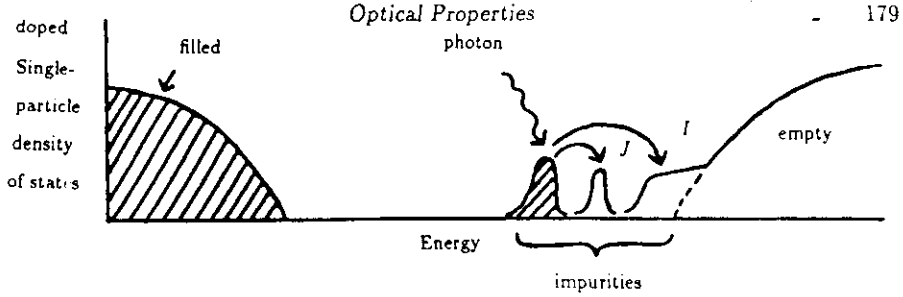

Figure 10: *Schematic diagram of the single-particle density of states of a doped insulator.*

	Nd_2CuO_{4-y}	$Ba_2YCu_3O_{6+y}$	La_2CuO_{4+y}	$La_{2-x}Sr_xCuO_{4+y}$
$E_I(meV)$	760±10	620±50	600±20	530±50
$E_C(meV)$	560	740	820	850
$E_G(meV)$	1450±50	1600±50	1800±50	1800±50
$E_J(meV)$	162±5	160±30	130±20	160±30
$E_R/2(meV)$	144±6	132±6	170±6	170±6
$J(meV)$	107±6	98±6	126 ±6	126±6
r(Å)	3.6	4.7	3.4	3.3
ϵ_L	6.3±0.3	4±0.5	5±0.3	5±0.3
f(per $100Cu$)	3.5±0.5 [0.5±0.5]	7 ±1	2±0.5 [0.5±0.5]	6±2

Table 1: *The peak energy E_I of the upper band in Figure 6, is near the ionisation energy of a charge bound to an impurity center as estimated by E_c using Equation 5. The magnitude of E_I indicates a deep impurity at a substantial fraction of the semiconducting energy gap E_G reported by Cooper 1990. The peak energy E_J of the lower band in Figure 6 may arise from an excitation as shown schematically in Figures 6-9. E_J is near half of the two-magnon Raman scattering peak $E_R/2$ and near the antiferromagnetic exchange energy, J, both reported by Sulewski (1990). The distance between the impurity center and a nearby, planar Cu atom, r, reported by Kwei (1989), Cava (1987), Siegrist (1987) and Chaillot (1989), is illustrated in Figures 7 and 11. The local dielectric constant ϵ_L is the value measured in undoped crystals in the frequency range near E_J and E_I (Thomas, 1990). The value, $f \equiv N/100$, is the fractional number of carriers added by doping, assuming a free electron mass and Equation 14. The numbers in brackets are the numbers for the undoped samples.*

The two peaks in Figure 6 can be fit with the functional form of a damped harmonic oscillator:

$$\sigma = \frac{\omega^2\omega_p^2\Gamma}{4\pi[\omega^2\Gamma^2 + (\omega^2 - E^2)^2]} \quad (6)$$

The plasma frequency ω_p^2 is related to the transition probability of one oscillator of mass m and charge e. It is fixed since the probability is 1 that the oscillator will be excited at some frequency. For n oscillators per unit volume, we have the plasma

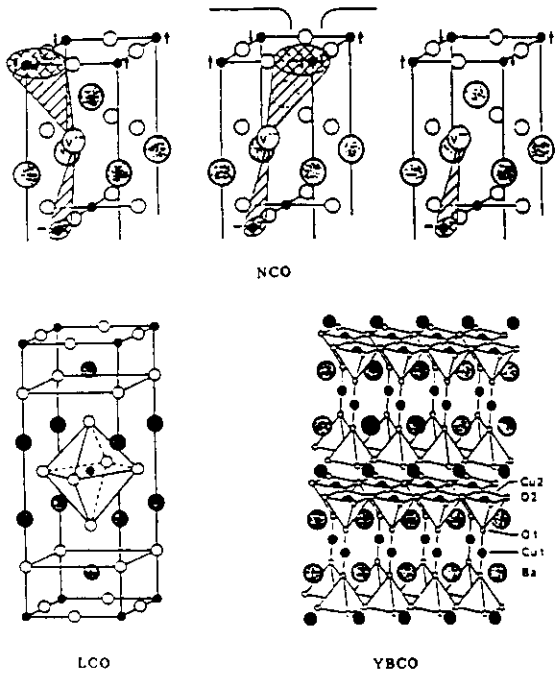

Figure 11: *Crystal structures of three cuprates, Kwei (1989); Cava (1987); Siegrist (1987) and Chaillout (1989).*

frequency:

$$\omega_p^2 = n4\pi e^2/m \ . \tag{7}$$

Fitting to the harmonic oscillator (Lorentzian) form gives the values of the line widths Γ and peak energies E listed in Table 1. The fractional number of carriers f is obtained from the prefactor ω_p^2 (a measure of the spectral weight).

The integrated area under these peaks is, by definition, the integrated rate of photon absorption. The area is directly proportional to the square of the plasma frequency ω_p of the excited charges for any functional form of the conductivity (the sum rule).

$$\int_0^\infty \sigma d\omega = \omega_p^2/8 \tag{8}$$

The units involved are

$$\sigma(\Omega.\mathrm{cm})^{-1} * 6 \times 10^{-4}(eV/(\Omega.\mathrm{cm})^{-1}) * \omega(eV) \propto \omega_p^2(eV)^2 \ . \tag{9}$$

From ω_p we can calculate a number of carriers N relative to some convenient volume. We shall use V_{Cu}, which we define as the unit cell volume V_{cell} normalised to the number of planar Cu atoms in it, N_{Cu}. This choice is helpful in comparing different crystal structures.

$$V_{Cu} = V_{cell}/N_{Cu} \ . \tag{10}$$

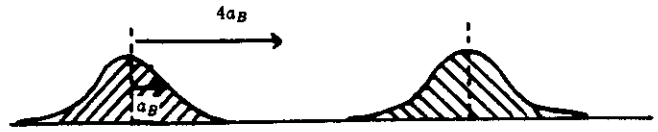

Figure 12: *Schematic representation of two wave functions with small overlap, representing the insulating state.*

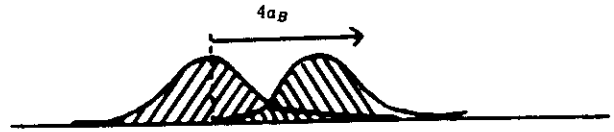

Figure 13: *Schematic representation of two wave functions with substantial overlap, representing the metallic state.*

For example

$$\begin{aligned} YBCO &: \ V_{Cu} \sim 170(\text{Å}^3)/2 = 85(\text{Å}^3), \\ LCO &: \ V_{Cu} \sim 100(\text{Å}^3). \end{aligned} \tag{11}$$

We can then write

$$N = (m/4\pi e^2) V_{Cu} \omega_p^2 \ . \tag{12}$$

If we assume the effective mass to be that of a free electron m_e we have the less general, but convenient, forms

$$n(\mathrm{cm}^{-3}) = 7.3 \times 10^{20} \omega_p^2(eV)^2 \tag{13}$$

$$N = 7.3 \times 10^{-4} V_{Cu}(\text{Å}^3) \omega_p^2(eV)^2 \ . \tag{14}$$

If there are two transitions from the same ground state, we can determine the fractional number of carriers involved in each f (related to a probability of excitation to each final state) as listed in Table 1; their sum is N. Our estimate of the dopant concentration y is half of this (corrected for N_{Cu}), in the case of oxygen dopants (or oxygen vacancies), since each added oxygen has 2 valence charges (2 holes bound to the O^{--} core).

At the density of carriers listed in Table 1, there is some small overlap of the bound state wave functions (which will contribute to the line width). We can picture the charge probability distribution in space (of Bohr radius, a_B) in a situation where there is very small overlap (Figure 12). At higher density, the overlap will increase and produce delocalisation of the charge (Figure 13).

The density, n_{MI}, or average separation, $(n_{MI})^{-1/3}$, at which this transition from metal to insulator occurs is given by the Mott criterion (Mott,1990):

$$(n_{MI})^{-1/3} = 4a_B \ . \tag{15}$$

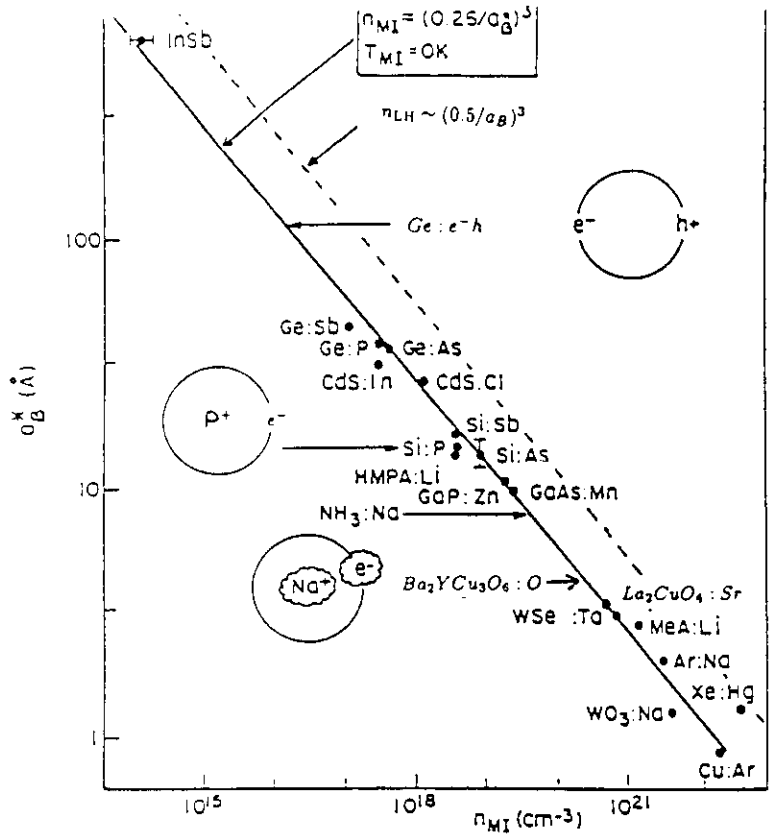

Figure 14: *Effective Bohr radii, a_B^*, as a function of metal–insulator transition density, n_{MI}, for a variety of materials as indicated. For example, P doping of a Si crystal is referred to as Si : P. The region of the transition line corresponding to the cuprates is indicated, based on rough estimates of the Bohr radii of 3 to 5Å. The figure is based on Edwards (1978).*

Some examples of the densities and Bohr radii at the metal-insulator transition are shown in Figure 14.

With increasing doping, the bands due to the dopants produce larger conductivities. We turn now to the metallic state, and ask to what extent these bands should still be considered. The conductivity added by doping in the insulating state is important because absorption (which is not understood) occurs near the same energy in the metallic and superconducting states.

4 Metallic state

4.1 Parts of the conductivity

We wish to understand the optically active states that occur in the metal. The main issue is how to formulate the problem. In general, there will be various contributions to the conductivity of the metal, just as in the insulator. Again, we expect the principal contributions to be:

$$\sigma = \sigma_{\text{phonons}} + \sigma_{\text{interband}} + \sigma_{\text{free}} + \sigma_{\text{impurities}} \tag{16}$$

In the metal, σ_{free} is no longer negligible. Since the free carriers come from the (overlapping) impurities, it is tempting to neglect $\sigma_{\text{impurities}}$. However, these finite frequency, direct, absorptions are a type of interband transition. It is a good approximation to retain the term $\sigma_{\text{interband}}$ when considering the appropriate energy region. We, therefore wish to consider retaining the low frequency "interband" transitions, $\sigma_{\text{impurities}}$. If we restrict ourselves to frequencies below E_{gap}, we can neglect $\sigma_{\text{interband}}$. The phonons are visible in insulating samples, but their direct absorption is small compared to the electronic contributions in the metals. The mass of the oscillators involved is large, so the phonon ω_P is small.

When can we neglect $\sigma_{\text{impurities}}$? This approximation is frequently used (Thomas,1988; Collins,1989; Schlesinger,1990 and Littlewood,1991) for analyzing relatively heavily doped crystals such as YBCO (90K). (The task then shifts to understanding the sources of scattering.) This "ordered crystal" or high density metal approximation ($n \gg n_{MI}$) is:

$$\sigma_{\text{metal}} = \sigma_{\text{free}} \,. \tag{17}$$

Another way of stating the question is at what density does the free electron approximation begin to work for the finite frequency conductivity? This question has been investigated by studying a series of samples in the metallic state with different doping levels (Suzuki,1989; Cooper,1989; Orenstein,1990 and Uchida, 1991). A summary of two of these sets of measurements is shown in Figure 15.

We suggest that the natural approximation for describing the curves at all but the highest density is to consider an approximation that retains $\sigma_{\text{impurities}}$. A resolved peak is visible in most of these curves at finite frequency (σ_{imp}), in addition to the peak centered at zero frequency (σ_{free}). Above $\omega = 1eV$, there is absorption which corresponds to the usual $\sigma_{\text{interband}}$.

The low density or disordered metal approximation ($n \geq n_{MI}$) is then:

$$\sigma_{\text{metal}} = \sigma_{\text{free}} + \sigma_{\text{imp}} \,. \tag{18}$$

4.2 Description of low-frequency interband conductivity

The similarity of σ_{imp} to that in the insulator is suggested by the spectrum. The position of the peak labelled by the arrows in the figure is near the peak labelled J in the insulator. The peak intensity grows with doping, but the shape, crudely, is

$$(\sigma_{\text{imp}})_{\text{metal}} \sim (\sigma_{\text{impurities}})_{\text{insulator}} \,. \tag{19}$$

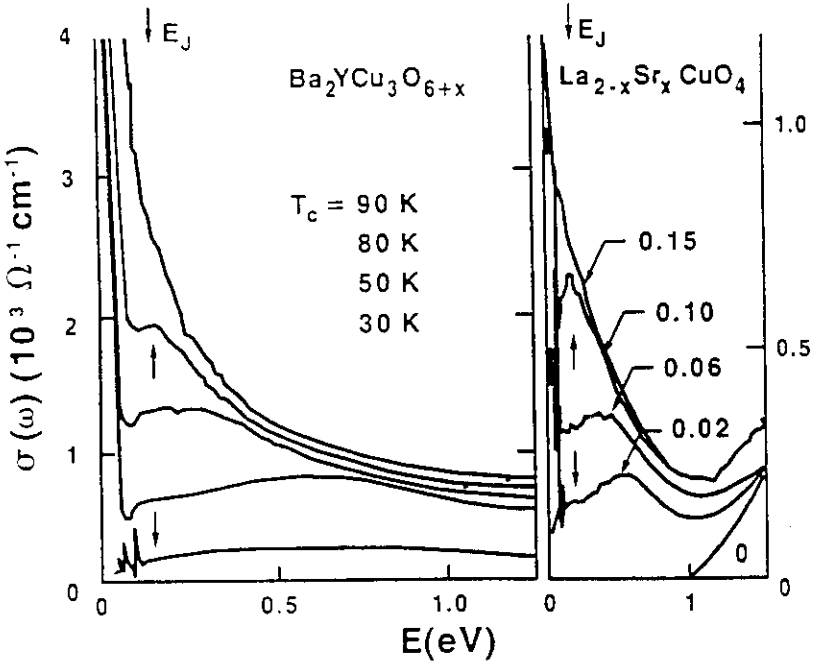

Figure 15: *The conductivity for 4 metallic samples of* YBCO *at a temperature of 100K, Orenstein (1990), and 4 metallic samples of* LSCO *at $T = 300K$, (Uchida,1991) with dopant levels as labelled, as a function of photon energy.*

The highest doped samples in Figure 15 present a situation that is less clear because 2 peaks are not resolved. In this case it seems reasonable to consider both the low density metal and high density metal approximations given above for describing σ. There is increased spectral weight near the energy E_J, which suggests including $\sigma_{\rm imp}$.

4.3 Low-density to high-density "transition"

We suggest that there exists a criterion for the crossover from a low density metal to a high density metal in the sense above (considering the system as a disordered, heavily doped semiconductor). As noted above, the Mott criterion, Mott (1990), indicates that the metal to insulator transition occurs at a density where only the tails of the wave functions overlap as shown in Figure 13. It seems reasonable that slightly above this density the typical wave function would still be well defined locally as shown in Figure 16. The wave functions would therefore retain some insulating character at finite frequency.

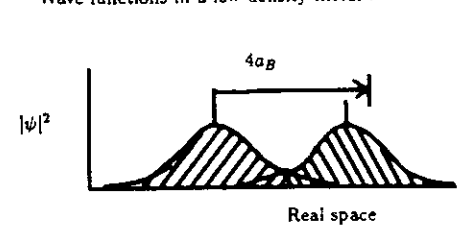

Figure 16: *Schematic representation of two wave functions in low density metal.*

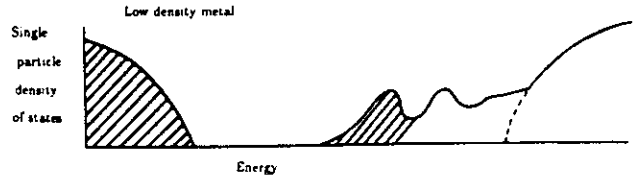

Figure 17: *Schematic representation of single particle density of states in low density metal.*

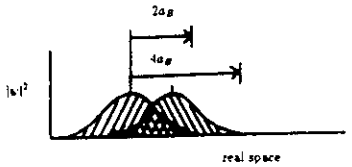

Figure 18: *Schematic representation of two wave functions in a high density metal.*

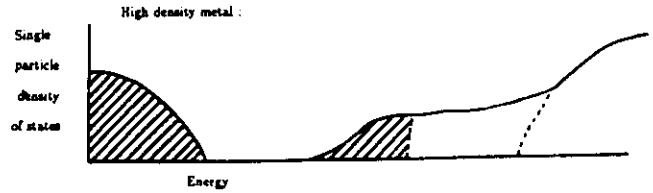

Figure 19: *Schematic representation of single particle density of states (high density metal).*

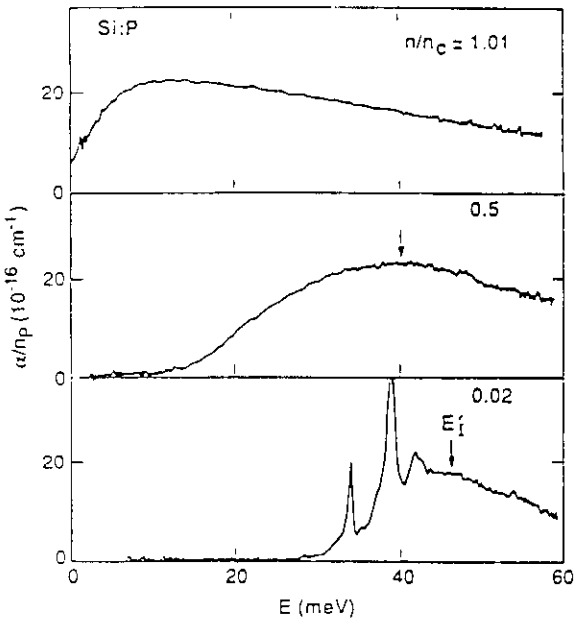

Figure 20: *The absorption coefficient normalised to the density of dopants (n_P) for three different crystals of Si doped with P, at $T = 10K$, as a function of photon energy. The two lower curves are insulators and the upper curve is a metal [unpublished data and Thomas (1981)].*

Figure 17 illustrates a possible single particle density of states in the low density metal. If the dopants were closer together, their average separation could become le s than their half width, and at this point, certainly, the typical sites would cease to be well defined even on a short length scale. (see Figure 18.) In this same regime of density, the low frequency interband transitions would wash out, as shown in Figure 19.

We therefore suggest the separation of twice the Bohr radius of the impurity as a criterion:

Low density metal to high density metal crossover, $(n_{LH})^{-1/3} \sim 2a_B$, $n_{LH} \sim 8n_{MI}$.

Something like this factor of 8 in density above n_{MI} describes the region above n_{MI} where $\sigma_{\rm imp}$ is apparently needed to describe the data shown in Figure 15. Here, large contributions that can be described as $\sigma_{\rm imp}$ seem to be a reasonable description of the optical conductivity in Figure 15. Similar insulating-like effects can be seen in the optical conductivity of other "conventional") heavily doped semiconductors such as crystalline *Si* doped with *P*. (see Figure 20.)

The metallic spectrum for *Si:P* shows a pronounced peak that is naturally interpreted as a contribution of the type $\sigma_{\rm imp}$. This peak is at the same energy as a weak transition in the insulator (Thomas, 1981) arising from the valley-orbit splitting of the ground state (forbidden in an isolated atom). This peak is thus similar to the peak labelled *J* above. The peak near the ionisation energy can be seen in the insulator, but is washed out in the metal (as in the cuprates).

4.4 Drude description of the free carrier conductivity

We turn now to approximations for describing $\sigma_{\rm free}$. The simplest approximation is the Drude model (Timusk ,1989). This model corresponds to elastic scattering by a fixed number of scatterers. This type of scattering may arise when defects are present which have no low frequency excitations. There are no low frequency interband transitions. It produces a conductivity of the simple form.

$$\text{Drude conductivity}: \qquad \sigma_{\rm free} = (\omega_p^2/4\pi\Gamma)/(1+\omega^2/\Gamma^2)\,; \qquad \sigma_{imp} = 0 \qquad (20)$$

In the limit of zero frequency, the inverse gives the resistivity.

$$\text{Drude dc resistivity}: \qquad \rho_{dc} = 4\pi\Gamma/\omega_p^2 = m\Gamma/ne^2 \qquad (21)$$

This simple scattering distribution gives a scattering rate, Γ, that is constant both in T and in ω. (see Figure 21).

It is now well established (Timusk,1989) that this form does not provide a good fit to either ρ_{dc} as a function of T or to σ as a function of ω. Figure 22 shows a comparison with the Drude model.

In early work on crystalline samples, the data were frequently compared to the Drude form (Timusk, 1989). This comparison is useful for a rough estimate of the spectral weight and the width. Examples of this comparison also serve to illustrate the calculation of the conductivity and dielectric constant ϵ from the measured reflectivity, R (or from the transmission, or from both).

Determining the real and imaginary parts of σ is straightforward experimentally (although there are important, systematic, experimental uncertainties, Orenstein,1990). The magnitude of the reflectivity R can be measured over a wide frequency range and extrapolated to $\omega = 0$ and $\omega = \infty$. The phase shift of the complex reflectivity can then be calculated using the Kramers-Krönig relation. An example of the use of this procedure is the first optical measurement (at room temperature) of a crystal of a composition that is close to a high temperature superconductor (Tajima,1988). (see Figure 23).

The Drude form is seen to be similar to σ at lower frequencies. On closer examination, particularly at lower T, the Drude form turns out to be a poor approximation. An example, Timusk (1988), is the first low temperature measurement of the absolute

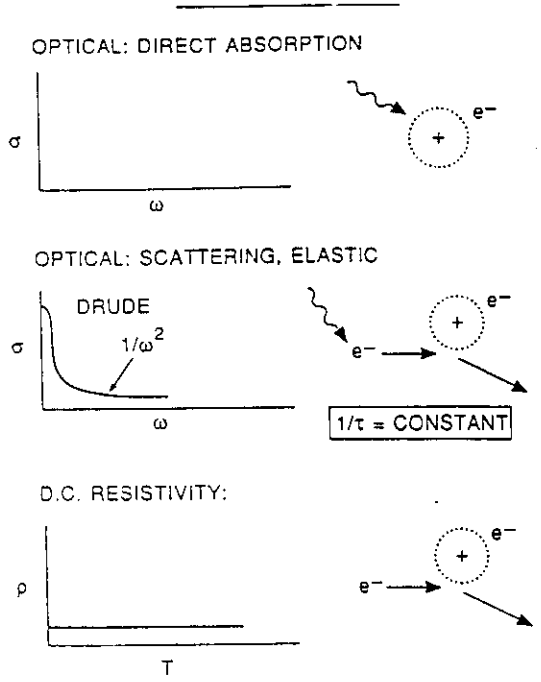

Figure 21: *Schematic representation of contributions to the conductivity in the Drude model.*

reflectivity, R, of crystals of YBCO (90K) with relatively high R at low T. Earlier measurements of pressed pellets, Timusk (1989), of reflectivity ratios of crystals (Schlesinger, 1987), and of the absolute R of inhomogeneous crystals (Thomas, 1987), are complicated to interpret. (see Figure 24.)

Five models for R are plotted as dashed lines in the left part of Figure 24. These models are calcı lated using the relation between the reflectivity and the complex conductivity or dielectric constant. The relation has a simple form in terms of ε:

$$R = |(\varepsilon^{1/2} - 1)/\varepsilon^{1/2} + 1|^2 . \tag{22}$$

There is also a useful approximate form (Hagen-Ruebens), at low frequency:

$$R = 1 - (8\pi\omega\Gamma)^{1/2}\omega_P \text{ for } \omega \ll \Gamma, \tag{23}$$

and another approximate form at intermediate frequencies (relaxation region)

$$R = 1 - 2\Gamma/\omega_P \text{ for } \Gamma \ll \omega \ll \omega_P . \tag{24}$$

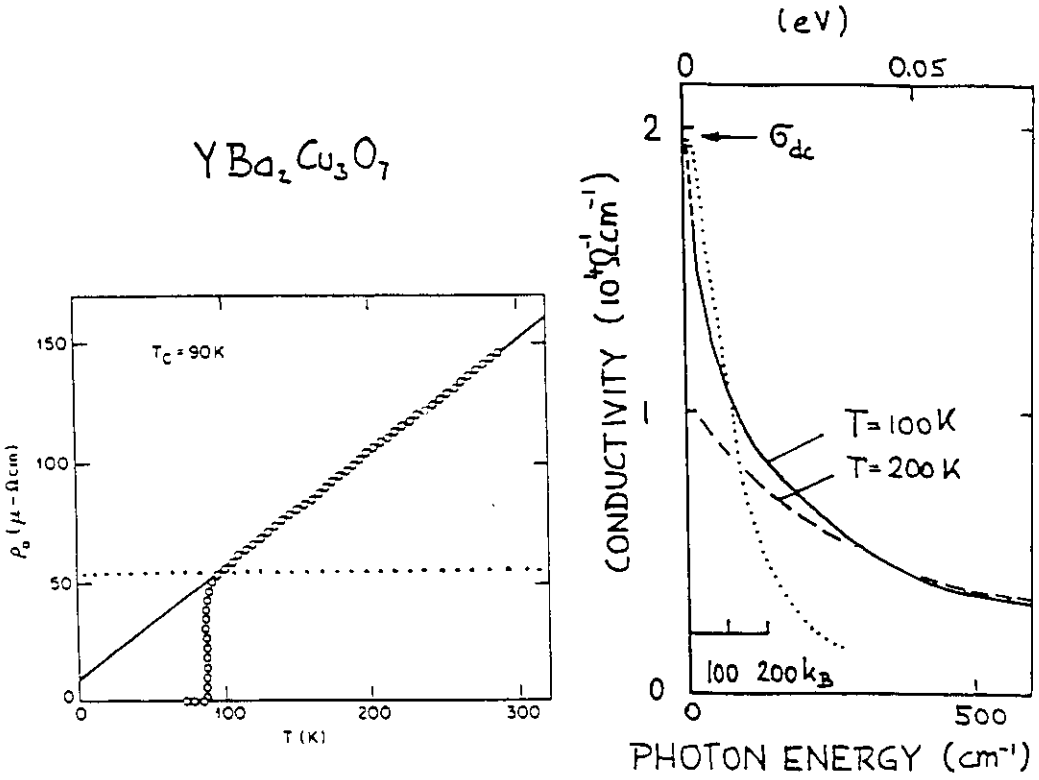

Figure 22: *On the left, the dc resistivity of a crystal of* YBCO *(90K) as a function of T. The open circles are data, the solid line is a linear fit, and the dashed line is the Drude theory (fitted to ρ_{dc} at T=100K, based on Orenstein (1990). On the right, conductivity of the same crystal as a function of frequency. The dashed curve is data recorded at T=200K, the solid curve at T=200K, and the dotted curve is the Drude theory fitted to σ_{dc} at $T = 100K$ and to the half width (Batlogg,1991 based on Orenstein 1990).*

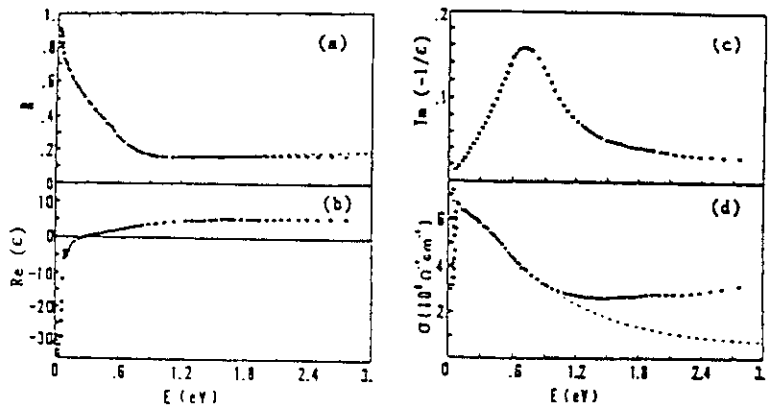

Figure 23: *Measured reflectivity (part (a)), as a function of frequency for a crystal of $LSCO(x = 0.2)$ at $T = 300K$. From this reflectivity the authors calculated the real part of the dielectric constant, $Re(\epsilon)$, (part (b)), as well as the imaginary part of the inverse, negative dielectric constant, $Im(-1/\epsilon)$, (part (c)), and the conductivity, (part (d)) (Tajima, 1988).*

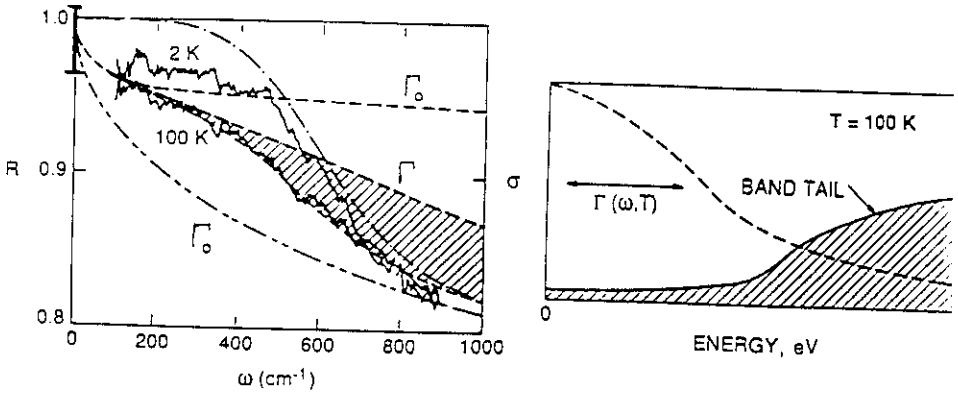

Figure 24: *Reflectivity (left part, solid curves) of aligned crystals of YBCO (90K) at two temperatures as a function of frequency. The dashed lines and shaded areas illustrate models for comparison with the data. The thick bar near $R = 1$ indicates our estimate of the uncertainty in the measured absolute value. Sketch (right part) of the possible corresponding conductivity. [Based on Timusk (1988).]*

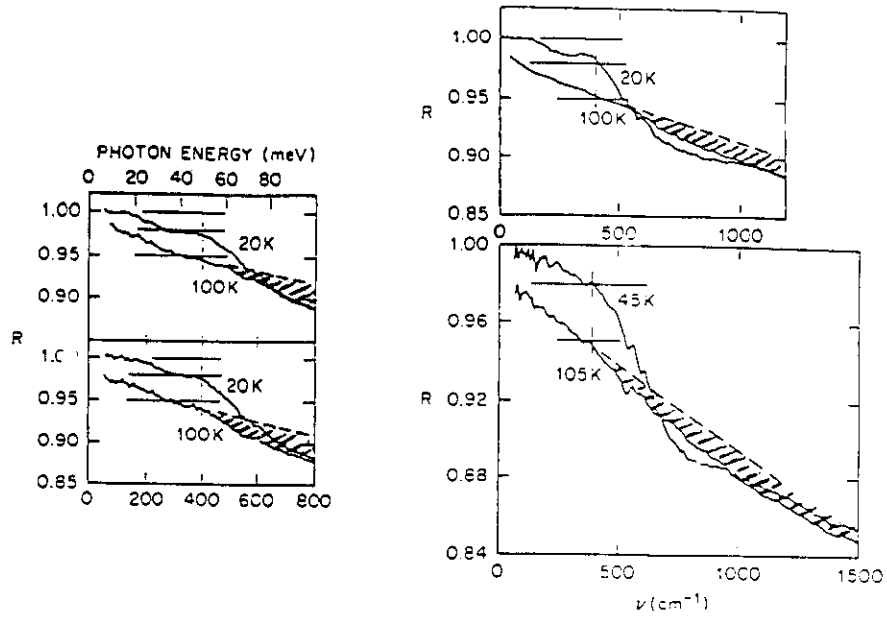

Figure 25: *Reflectivity of crystals of YBCO (90K) as a function of frequency at two low temperatures, as labelled. These temperatures are just above, and just below the superconducting transition temperature. The two left graphs [Kamaras, 1990] and the upper right graph [Schutzmann, 1989], are data from films, the lower right graph [Collins, 1989] is a result for a crystal.*

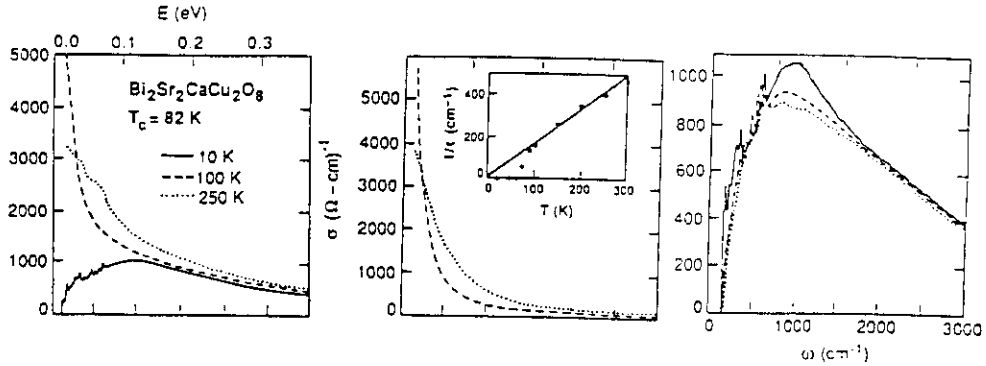

Figure 26: *Left part, measured conductivity as a function of frequency for a crystal of BSCCO at three temperatures. Middle part, Drude forms fitted at low ω. Inset, values of $1/\tau$ (Γ in our notation) from the Drude fits. Right part, the difference (σ_{imp} in our notation) between the Drude fits and the measured conductivity (Romero 1991).*

In Figure 24, three curves are drawn, assuming $\sigma = \sigma_{free}$ (i.e. $\sigma_{imp} = 0$). Each of these uses a different estimate of the scattering rate, based on the approximate form:

$$\Gamma = \Gamma_0 + 2\pi\lambda(\omega + \pi T) \; . \tag{25}$$

If this form were to hold (λ non-zero) in the limit as ω and T go to zero, the electronic fluid would only marginally be a Fermi liquid (Varma 1989; Littlewood 1991). The fits use different values of the constants, Γ_0, λ, and c:

$$\begin{aligned} \lambda \quad &= 0, \quad \Gamma_0 \quad \text{fit for } \omega \lesssim 200 cm^{-1} \; . \\ \lambda \quad &= 0, \quad \Gamma_0 \quad \text{fit for } \omega \lesssim 900 cm^{-1} \; . \\ \Gamma_0 \quad &= 0, \quad \lambda \quad \text{fit for } \omega \lesssim 900 cm^{-1} \; . \end{aligned}$$

The main point from these comparisons is that the models do not provide adequate anproximations to these data. The first two are Drude, labelled Γ_0 in the figure. The third (labelled Γ) is preferable since it provides a reasonable description of the linear *dc* resistivity (*see*, for example, Figure 22). However, the shaded area emphasises the extra absorption that appears to be present in the data. As an alternative description, we turn again to the two component conductivity, $\sigma = \sigma_{free} + \sigma_{imp}$. This case is illustrated Figure 24. The dashed line that is hard to distinguish from the data on the left is a sum of the Lorentzian form for σ_{imp} (the band tail) and the Drude form for σ_{free}. Empirically, the free carrier part becomes narrower with decreasing T (Γ decreases) (Orenstein,1990), and some of the spectral weight will go into a delta function at $\omega = 0$ in the superconducting state. An approximation for the R data at T=2K is the dash-dot curve shown which replaces σ_{free} with the delta function, and uses the same band tail (Timusk,1989). Similar measurements of R have been carried out by several groups, as shown in Figure 25. The results in Figures 24 and 25 show that the measurements are similar, but not the same under close examination. The shaded areas indicate the possible usefulness of an approximation including σ_{imp}. Another example of fitting the conductivity with two parts has been carried out for $Ba_2Sr_2CaCu_2O_8$ (BSCCO), as shown in Figure 26.

4.5 A Model of the Scattering Rate

The analysis of σ_{free} above indicates that it is useful to consider the scattering rate Γ as a variable (Holstein,1954 and Allen,1971) rather than a constant. It may be easier to guess the scattering mechanism from an examination of Γ, rather than σ or R. To do this, we need to use both the real and the imaginary parts of the conductivity. We use the notation :

$$[\sigma_{complex}]_{free} \equiv [\sigma + i\sigma_I]_{free} \tag{26}$$

and we define the variables Γ and m^*/m using

$$[\sigma + i\sigma_I]_{free} \equiv (\omega_p^2/4\pi)/[\Gamma - i(m^*/m)\omega] \; . \tag{27}$$

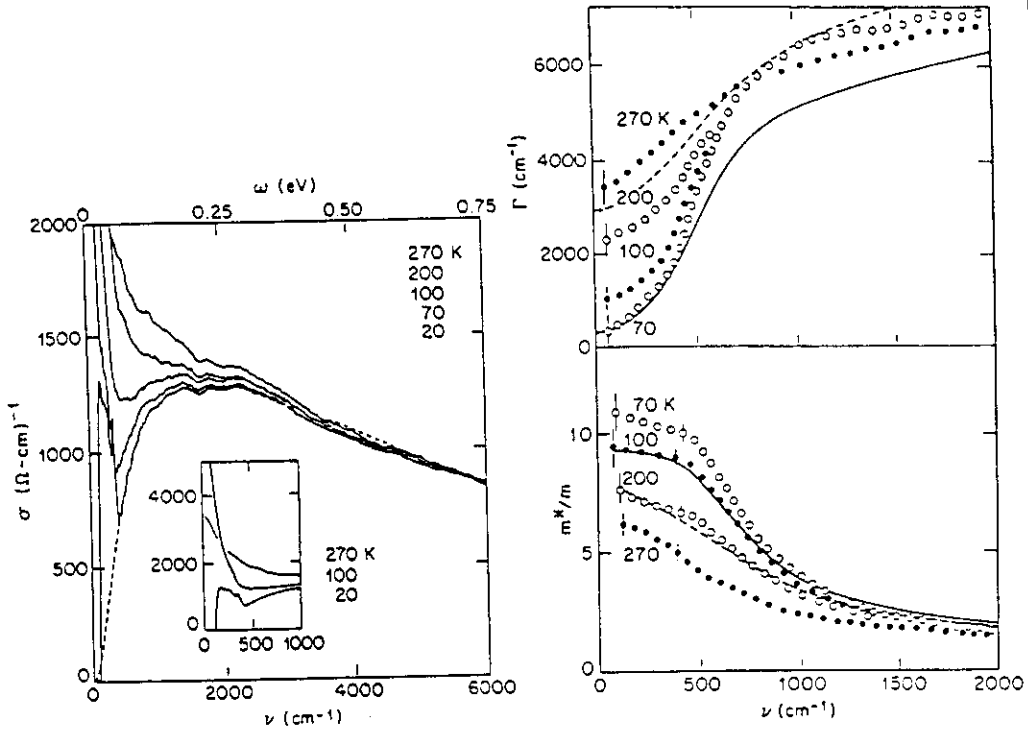

Figure 27: *Left, conductivity of a crystal of* YBCO *(50K) for five values of temperature as a function of frequency. The dashed line is a sketched estimate of the low frequency part of a possible band of direct absorption (σ_{imp}). Right, effective scattering rate and effective mass (from ω_p^2) as a function of frequency for the same crystal. The right figure is constructed on the dubious assumption that all of the conductivity is from free carriers [Thomas (1988)].*

This allows us to solve for Γ and for m^*/m:

$$\Gamma = (\omega_p^2/4\pi)[(\sigma/\sigma_I^2)/(1 + (\sigma/\sigma_I)^2)]_{free} \tag{28}$$

$$(m^*/m) = (\omega_p^2/4\pi)/[\omega\sigma_I(1 + (\sigma/\sigma_I)^2)]_{free} \; . \tag{29}$$

Figure 27 is an example of the use of this reformulation on the entire conductivity.

If there is a band of direct absorption, as seems likely from inspection of the conductivity in the left part of the figure, then the analysis in the right part should not have been done on the entire σ. As we have emphasised (*e.g.* , by our subscript "free"), the experimental difficulty comes back to our main point: how to decompose the measured σ into free and interband parts (particularly low frequency interband from the dopants)? Is $\sigma_{measured}$ equal to σ_{free} or is it equal to $\sigma_{free}+\sigma_{imp}$? Since we are unsure how to separate the parts of σ, we are stuck, and can only make guesses. One reasonable set of guesses involves assuming a scattering distribution, that describes ρ_{dc} and $\Gamma(\omega = 0)$, and using that guess to calculate σ_{free}. An important approximation [Migdal (1958)] commonly used is to calculate the electron (or hole) quasiparticle scattering rate (or imaginary part of the self energy) and assume that this rate is similar to the transport scattering rate. An example (Thomas, 1988 and Orenstein,1990) of this procedure is to assume a "box" shaped distribution of scattering excitations (independent of momentum) which is a constant, $\alpha^2F \equiv (\lambda/2)ln(\omega_n/\omega_e)$ from a frequency ω_e to ω_n, as shown in the inset to Figure 28.

The average scattering frequency, Ω_0, is given by

$$\Omega_0 = (2/\pi)\int_0^\infty \alpha^2 F dw \ , \tag{30}$$

and the limiting forms are the following:

$$\begin{aligned} \Gamma_{dc} &= 2\pi\lambda T \quad \text{for } \omega = 0, T \gg \Omega_0 \\ \Gamma &= 2\pi\lambda T \quad \text{for } \omega \gg \Omega_0 \end{aligned}$$

The curves in Figure 28 show the results for Γ.

If we can agree on an estimate of ω_p^2 for the free carriers, we can determine λ experimentally (Thomas 1988, Orenstein 1990) from ρ_{dc}.

$$\begin{aligned} \text{For} \quad \omega_p &= 1.4eV, \\ \lambda &= 0.4 \ . \end{aligned}$$

The box-shaped scattering distribution is reasonable since it vaguely resembles the phonon density of states and therefore provides one likely component of the scattering (Timusk,1991). An example, for YBCO , has been measured by neutron scattering (Figure 29).

We reemphasise that models of the scattering of the free carriers should be compared only to the relevant part of the measured conductivity.

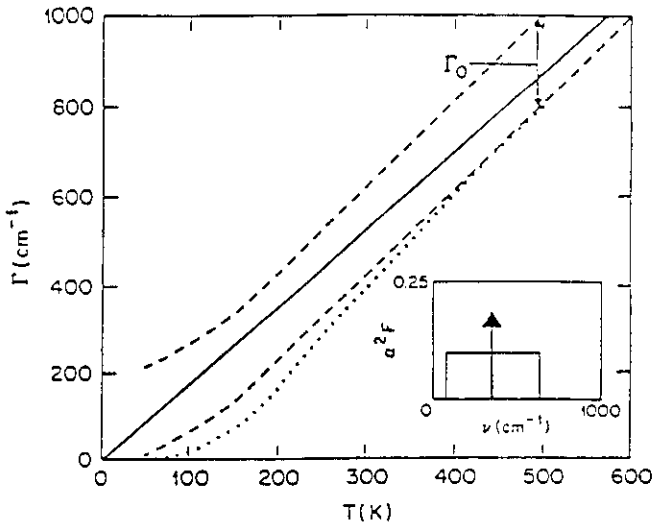

Figure 28: *Calculated scattering rate as a function of temperature (lower dashed line). The scattering distribution assumed is shown in the inset. The lower dotted line is an approximate form. The solid line is $2\pi\lambda T$. The upper dashed line assumes a constant, additional scattering, Γ_0.*

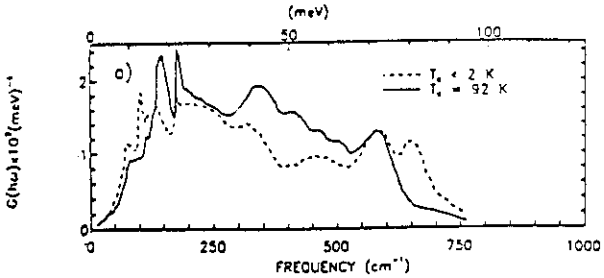

Figure 29: *Neutron scattering intensity as a function of frequency for two crystals, YBCO(0K) dashed line and YBCO (90K), (solid line) (reprinted from Timusk,1991).*

5 Superconducting state

The discussion of the "normal" state presented above already covers the key considerations that should be emphasised regarding the superconducting state. The figures presented above include a number of important measurements of this state. These data have been interpreted (Cooper,1989 and Orenstein,1990) as indicating a superconducting energy gap that is small, (Thomas,1988) a gap that is large, (Schlesinger,1990) and a gap that is unobservable (Pham,1990; Kamaras,1990; Timusk,1991 and Pham,1991). Given the fundamental uncertainties that we have about the "normal" metallic state, it is to some extent premature to discuss the superconducting state. Instead this author shall present an empirical summary of measurements on approximately a dozen samples and point out three features: 1) A "weak" edge, E_ω near $3.5T_c$; 2) a "strong" edge E_s, at a larger energy, and 3) a tail of absorption that extends all through this energy region. The discussion is given in the captions of Figures 30–37.

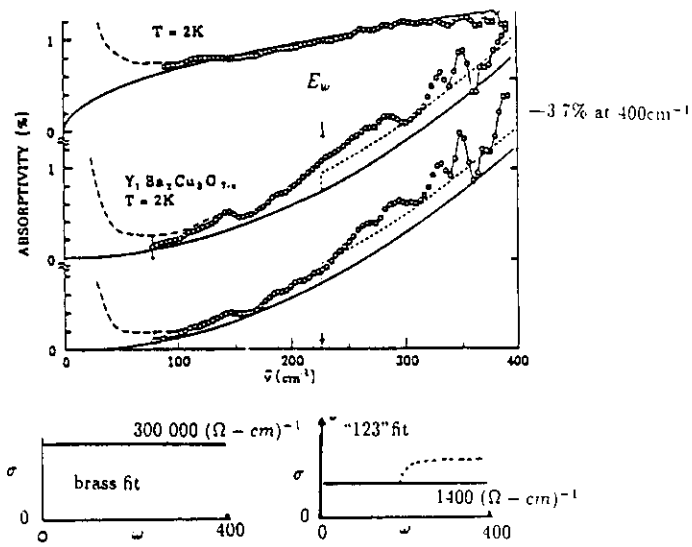

Figure 30: *Evidence of a tail of low frequency absorption intensity in the superconducting state and a comparison with a possible weak energy edge ($E_\omega = 3.5T_c$). This latter feature is hard to see. The absorptivity $1 - R$ is measured (open circles and dashed line at low frequency) as a function of frequency, in two twinned crystals of* YBCO *(90K), (and a brass sample for reference) at $T = 2K$ (Pham, 1990). The upturn at low frequency is believed spurious. The lower figures are sketches to explain the fits: solid lines are constant conductivities, dashed lines at higher frequency are possible indications of a small gap.*

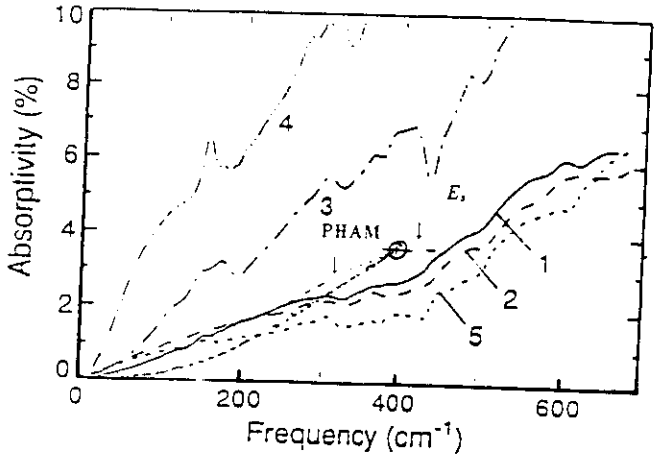

Figure 31: *Evidence that the low frequency absorption below T_c varies with disorder in the sample, and evidence of a strong absorption edge E_s, near 430cm^{-1}. The absorptivity is plotted as a function of frequency for five films (twinned) of YBCO(90K, at T = 1.5K, Miller (1991) preprint.*

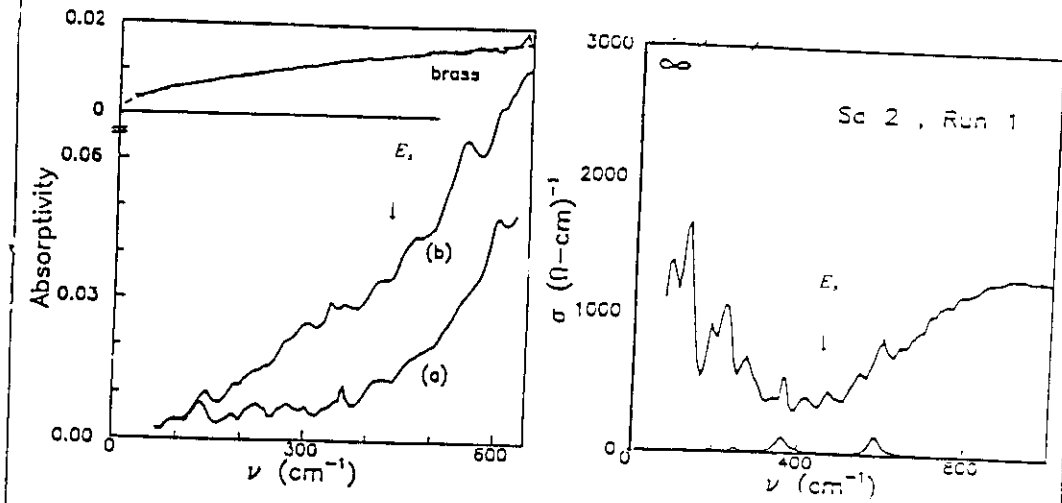

Figure 32: *Evidence of low frequency absorption and an edge E_s in an untwinned crystal. The absorptivity as a function of frequency is shown for the a-axis (a) and the b-axis (b) of a crystal (Welp, 1990) of YBCO (90K), and for a brass reference, at T = 2K (Pham, 1991). The corresponding a-axis conductivity derived from this absorptivity (upper solid curve, right graph) is also shown, along with the direct absorption observed from phonons in an insulating sample of YBCO (0K) (lower bumps).*

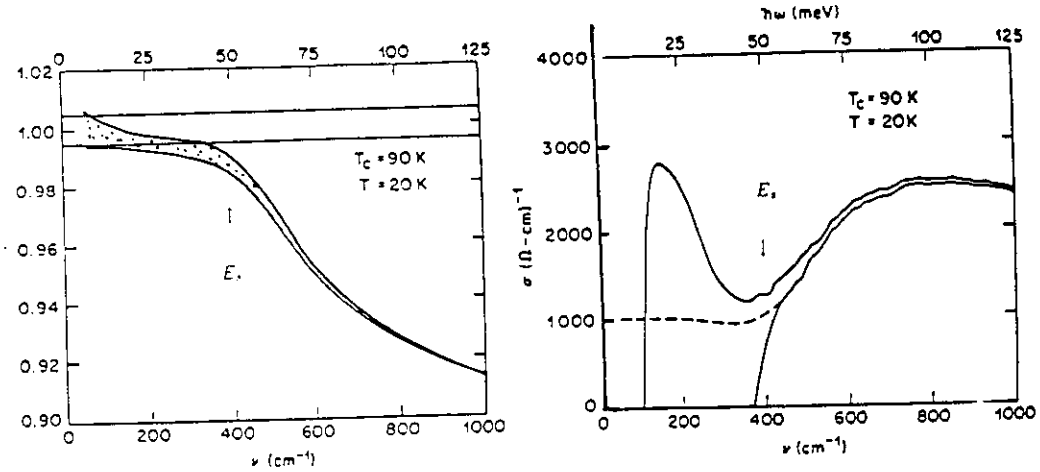

Figure 33: *Evidence of a strong absorption edge, E_s, near 400cm^{-1}. Reflectivity (shaded area, left graph) as a function of frequency for a twinned crystal of YBCO (90K) at $T = 20K$, Orenstein (1990). The 1% estimated uncertainty in the absolute value of R is indicated by the horizontal, solid lines near $R = 1$. Some possible conductivity curves that can be derived from the measured R within the uncertainties are shown in the right graph, (Orenstein, 1990).*

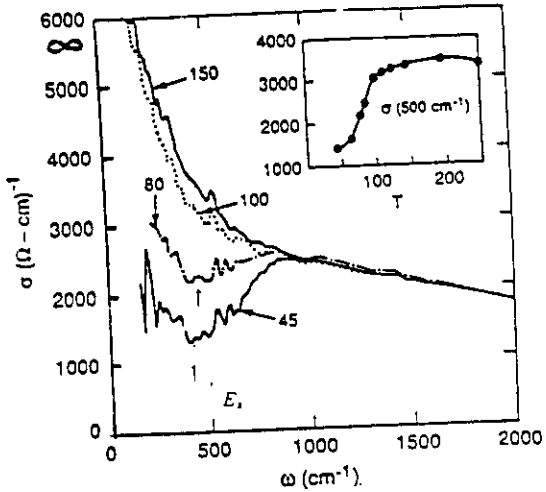

Figure 34: *Evidence that the feature E_s does not shift appreciably with T and is indistinct in this sample above T_c. The Gap might be large, based on the T-dependence. The conductivity is plotted as function of frequency for a twinned crystal of YBCO (90K) at four temperatures as labelled (main plot) and at a fixed frequency as a function of T (inset) (Collins, 1989).*

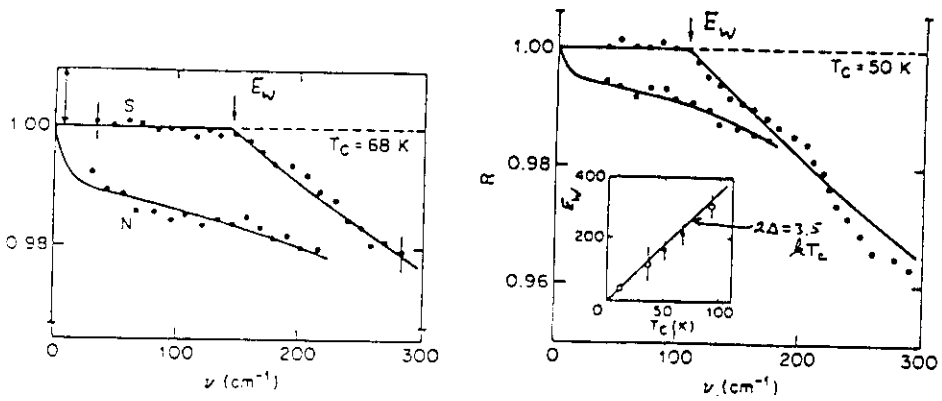

Figure 35: *Evidence of a weak edge, E_w, at lower energy than E_e. The reflectivity is shown as a function of frequency for a twinned crystal of YBCO (68K) (left graph) at $T = 10K$ (upper dots, labelled S) and at $T = 90K$ (lower dots, labelled N). The arrow near $R = 1$ indicates an estimate of the uncertainty in the absolute value of R, the solid lines are guides to the eye to make the scatter in the data look smaller. The right graph shows the same results for a crystal of YBCO (50K). The inset shows these two values of E_w as solid dots along with other observed weak edges from $Ba_{1-x}Pb_xBiO_3$, $La_{2-x}Sr_xCuO_4$ and YBCO (90K) pressed pellets (with error bars that may be too small) as a function of the superconducting transition temperatures, T_c (Thomas, 1988).*

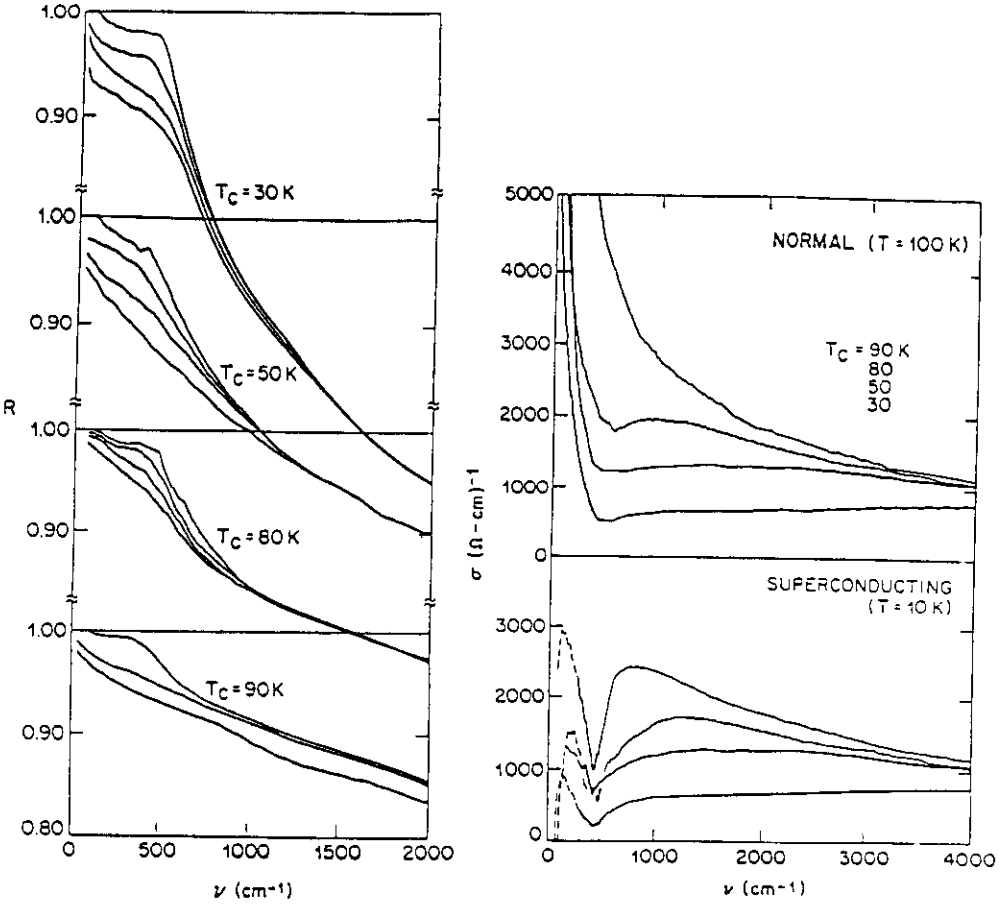

Figure 36: *Left: Evidence that E_s (the "knee" in R just below 500cm^{-1}) does not change in energy in crystals with different values of T_c, and that the "knee" is present above T_c. The R plotted as a function of frequency for four crystals of YBCO (values of T_c indicated) at a series of temperatures (uppermost curve for each crystal is below T_c, lower curves are mostly above T_c) (Orenstein, 1990). Right: Conductivity, derived from the measured R shown in Figure , as a function of frequency for four twinned crystals of YBCO with values of T_c listed, in the "normal" state at $T = 100K$, upper part. The lower part shows the same four crystals at $T = 10K$. The dashed curves at low frequency indicate parts of the curves that are extremely uncertain (Orenstein, 1990).*

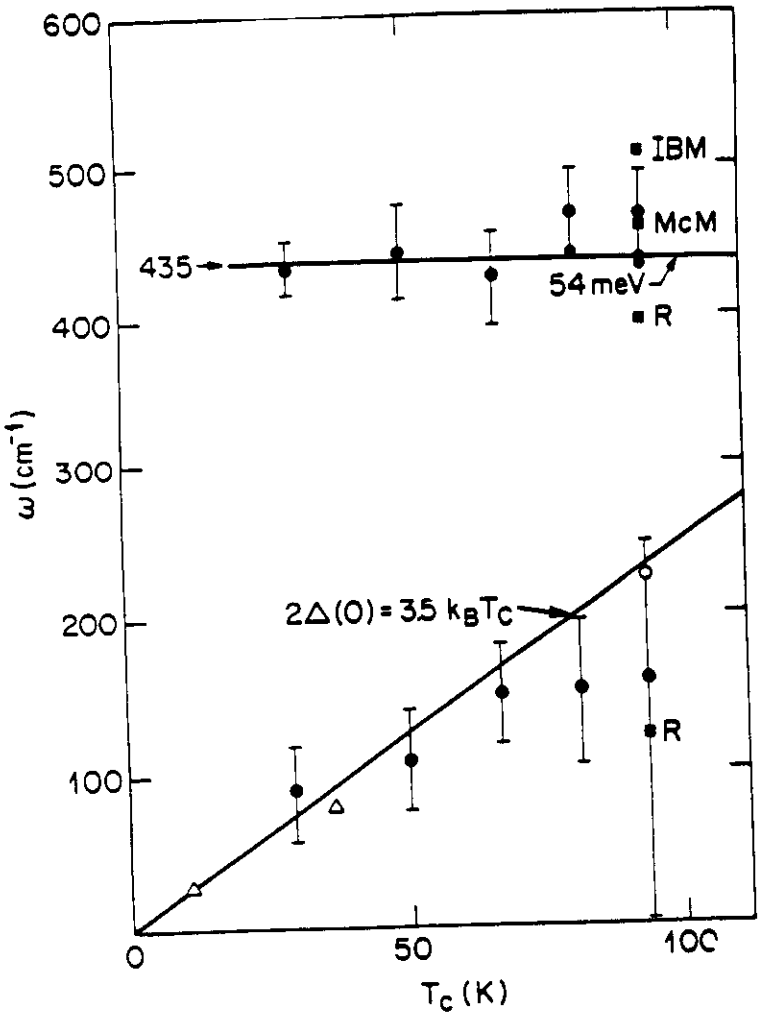

Figure 37: *Summary of values of the strong absorption edge, E_s (upper points) and the weak edge, E_w (lower points) as a function of T_c for different materials. The upper points are from YBCO crystals: solid circles from Thomas (1988) and Cooper (1989); "IBM", solid square, from Collins (1989); "McM" from Timusk (1988); "R" from Schützman (1989). The lower solid points are some YBCO crystals (same notation) and the open points are $Ba_{1-x}Pb_xBiO_3$ crystals, $La_{2-x}Sr_xCuO_4$ and YBCO(90K) pressed pellets summarised in Timusk (1989).*

References

Batlogg B, 1990. In-High Temperature Superconductivity, K S Bedell, *et al.* (eds) (Addision-Wesley) 37.

Batlogg B,1991. *Physics Today* (in press).

Bednorz J G, Müller K A, 1986. *Z. Phys.* **B64** 189.

Budnick J I, *et al.* 1988. *Europhys. Lett.* **5** 651.

Cava R J, van Dover R B, Batlogg B and Rietman E A, 1987. *Phys. Rev. Lett.* **58** 408.

Cava R J, Santoro A, Johnson, Jr. D W, and Rhodes W W, 1987. *Phys. Rev.* **B35** 6716.

Chaillout C, Cheong S-W, Fisk Z, Lehmann M S, Marezio M, Morosin B and Schirber J E, 1989. *Physica C* **158** 183.

Collins R T, Schlesinger Z, Holtzberg F, Chaudari P and Feild C, 1989. *Phys. Rev.* **B39** 6571.

Cooper S L, Thomas G A, Orenstein J, Rapkine D H, Capizzi M, Timusk T, Millis A J, Schneemeyer L F and Waszczak V J,1989. *Phys. Rev. B.* **40** 11358.

Cooper S L, Thomas G A, Millis A J, Sulewski P E, J Orenstein, Rapkine D H, Cheong S-W and Trevor P L, 1990. *Phys. Rev.* **B42** 10785.

Edwards P P, Sienko M J, 1978. *Phys. Rev. B* **17** 2575.

Forro L, Carr G L, Williams G P, Mandrus D and Mihaly L, 1990. *Phys. Rev. Lett.* **65**, 1941.

Ginder J M, Roe M G, Song Y, McCall R P, Gaines J R, Ehrenfreund E and Epstein A J, 1988. *Phys. Rev.* **B37** 7506.

Harshman D R, Aeppli G, Espinosa G P, Cooper A S and Remeika J P, E J Ansaldo, Riseman T M and Williams D L, Noakes D R, Ellman B and Rosenbaum T F, 1988. **38** 852.

Heyen E T, Kliche G, Kress *N*, Konig W, Cardona M, *et al.* 1990. *Sol. St. Comm.* **74** 1299.

Kamaras K, Herr S L, Porter C D, Tache N, Tanner D B, Etemad S, Venkatesan T, Chase E, Inam A, Wu X D, Hegde M S and Dutta B, 1990. *Phys. Rev. Lett.* **64** 84.

Kwei G W, Cheong S-W, Fisk Z, Garzon F H, Goldstone J A and Thompson J D, 1989. *Phys. Rev.* **B40** 9370.

Littlewood P B, Varma C M, 1990, *Proc. Int'l. Conference on Theory of High-T_c Superconductors* **JINR** (Dubna USSR) p.178.

Luke G M, Le L P, Sternlieb B J, Uemura Y J, Brewer J H, Kadono R, Kiefl R F, Kreitzman S R, Riseman T M, Stronach C E, Davis M R, Uchida S, Takagi H, Tokura Y, Hidaka Y, Murakami T, Gopalakrishnan J, Sleight A W, Subramanian M A, Early E A, Markert J T, Maple M B and Seaman C L, 1990. *Phys. Rev.* **B42** 7981.

Mihailovic, D C, Foster M, Voss K and Heeger A J, 1990. *Phys. Rev.* **B42** 7989.

Miller D, Richards P L, Etemad S, Inam A, Venkatesan T, Dutta B, Wu X D, Oem C B, Geballe T H, Newman N, Cole B F (preprint).

Misiewicz, J, Becla P, Isaacs E D, Wolff P A, Heiman D, Ram-Mohan L R and Wrobel J M, *J.Appl.Phys.* **63** 2396; Lang I G, Firsov Y A, 1963. *Sov. Phys. JETP* **16** 1301; Emin D, 1975. *Adv.Phys.* **24** 305.

Moser F, Matz D and Lyn S, 1969. *Phys. Rev.* **182** 808.

Mott, N F, 1990. Metal-Insulator Transitions (Taylor and Francis).

Orenstein, J, Thomas G A, Millis A J, Cooper S L, Rapkine D H, Timusk T, Schneemeyer L F and Waszczak J V, 1990. *Phys. Rev.* **B42** 6342.

Pham, T, Drew H D, Moseley S H, Liu J Z, 1990. *Phys. Rev.* **B41** 11681.

Pham T, Lee M W, Drew H D, Welp U, Fang Y, 1991 (preprint).

Phillips J C, 1989. Physics of High T_c Superconductors (Academic Press).

Preyer N W, Birgeneau R J, Chen C Y, Gabbe D R, Jenssen H P, Kastner M A, Picone P J and Thio T, *Phys. Rev.* **B39** 11563.
Rabe K, Bhatt P N, 1990. *Proc. 20th Int. Conf. Phys. Semiconductors* (in press).
Romero, D, 1991. *Physics Today* (in press).
Schlesinger Z, Collins R T, Kaiser D L and Holtzberg F, 1958. *Phys. Rev. Lett.* **59**.
Schlesinger Z, Collins R T, Holtzberg F, Feild C, Koren G and Gupta A, 1990a. *Phys. Rev.* **B41** 11237.
Schlesinger Z, Collins R T, Holtzberg F, Feild C, Blanton S H, Welp U, Crabtree G W, Fang Y and Liu J Z, 1990b. *Phys. Rev. Lett.* **65** 801.
Schüzmann, J, Case W, Keller J, Renk K F, Roas B, Schultz L and Saemann-Ischenko G, 1989. *Europhys. Lett.* **8** 679.
Shraiman B, Millis A, 1991. (private comm.).
Siegrist T, Sunshine S, Murphy D W, Cava R J and Zahurak S M, 1987. *Phys. Rev.* **B35** 7137.
Sulewski P E, Fleury P A, Lyons K B, Cheong S-W and Fisk Z, 1990. *Phys. Rev.* **B41** 225.
Suzuki M, 1989. *Phys. Rev.* **B39** 2312.
Tajima S, Uchida S, Ishii H, Takagi H, Tanaka S, Kawabe U, Hasegawa H, Aita T and Ishiba T, 1988. *Mod. Phys. Lett* **B1** 353.
Takagi, H, Uchida S and Tokura Y, 1989. *Phys. Rev. Lett.* **62** 1197.
Talliani C, Zamboni R, Ruani G, Matacotta F C and Pokhodnya K I, 1988. *Sol. St. Comm.* **66** 487.
Thomas, G A, Capizzi M, DeRosa F, Bhatt R N, and Rice T M, 1981. *Phys. Rev.* **B23** 5472.
Thomas, G A, Cappizi M, Orenstein J, Rapkine D H, Schneemeyer L F, Waszczak J V, Millis A J and Bhatt R N, 1987. *Jpn. J. Appl. Phys. Supp.* **26** 2044.
Thomas G A, Orenstein J, Rapkine D H, Capizzi M, Millis A J, Bhatt R N, Schneemeyer L F and Waszczak J V, 1988. *Phys. Rev. Lett.* **61** 1313.
Thomas G A, Rapkine D H, Cooper S L, Cheong S-W, Cooper A S, 1991. *Phys. Rev. B* (in press).
Timusk, T, Bonn D A, Greedan J E, Stager C V, Garrett J D, O'Reilly A H, Reedyk M, Kamaras K, Porter C D, Herr S L and Tanner D B, 1988. *Physica C* **153-55** 1744.
Timusk T, Tanner D B, 1989. In Physical Properties of High Temperature Superconductors I, D Ginsberg (ed) (World Scientific) p.339.
Timusk T, Porter C D and Tanner D C, 1991. *Phys. Rev. Lett.* **66** 663.
Uchida S, Ido T, Takagi H, Arima T, Tokura Y and Tajima S, 1991. *Phys. Rev.* **B43** (7942).
Varma C M, Littlewood P B, Schmitt-Rink S, Abrahams E and Ruckenstein A E, 1989. *Phys. Rev. Lett.* **63** 1996; *ibid.* 1990. **64** 497 (E).
von Szczepanski, K J, Rice T M, and Zhang F C, 1989. *Europhys. Lett.* **8** 797.
Welp U, Fleshier S, Kwok W K, Downey J, Fang Y, Crabtree G W and Liu J Z, 1990. *Phys. Rev.* **B42** 10189.
Wu M K, Ashburn J R, Torng C J, Hor P H, Meng R L, Gao L, Huang Z J, Wang Q Y and Chu C W, 1987. *Phys. Rev. Lett.* **58** 908.